Bloch theorem in cylindrical coordinates and its application to a Bragg fiber

Akira Kitagawa* and Jun-ichi Sakai†
Department of Photonics, Faculty of Science and Engineering, Ritsumeikan University, Noji-Higashi, Kusatsu City, Shiga 525-8577, Japan
(Received 4 June 2009; published 1 September 2009)

We study the description of the Bloch theorem in the cylindrically periodic structure and we show that it is valid in a good approximation except for the neighborhood of the origin. The cylindrical Bloch theorem is applied to the analysis of a Bragg fiber, a kind of photonic bandgap fibers. It is confirmed that the above exception does not prevent us from using the theorem for a practical use. We show a procedure to obtain the propagation constant and electromagnetic fields of the TE mode in the Bragg fiber. In the present scheme, electromagnetic fields are genuinely treated as cylindrical waves, namely, Bessel functions without the asymptotic expansion. Then we can obtain a clear mathematical description of the Bragg fiber and investigate its physical properties. The present theory gives a criterion to design generalized Bragg fibers.

DOI: 10.1103/PhysRevA.80.033802 PACS number(s): 42.70.Qs, 42.81.Qb, 03.50.De

I. INTRODUCTION

In a periodic structure, a wave is subject to the Bragg diffraction, which is a fundamental physical process. To analyze the wave function in such a stratified material, the Bloch theorem [1,2] has been applied. This theorem is originally intended to use in the Cartesian coordinates and the Bloch wave number is determined from the periodic boundary condition with adequately long periodicity. As an application in fiber optics, a Bragg fiber has been proposed [3], which has a hollow core and a periodically alternating cladding of high and low refractive indices.

Since the first proposal of photonic bandgap in 1987 [4], the photonic crystal has been under intense study. It is well known that the electromagnetic field of specific wavelength is forbidden in suitably designed photonic crystals. This property is effective to confine the electromagnetic fields to a specific region. In 1995, the photonic crystal fiber was proposed [5], in which the refractive index is controlled by the periodicity of its inner structure, such as arrangement of air holes [6]. In particular, photonic crystal fibers where light is confined to the core due to the photonic bandgap are referred to as the photonic band-gap fibers.

The photonic bandgap fiber has a lot of preferable properties to the conventional optical fibers based on the total internal reflection at the core-cladding interface. Since extremely low-loss propagation is expected in photonic bandgap fibers with a hollow core, wavelength region other than telecommunication wavelength can be used. Furthermore, small nonlinear effects are remarkable features for various applications.

Recently, research on Bragg fiber has revived as a kind of photonic bandgap fibers. It has been studied analytically [7–10], semianalytically [11], and numerically [12,13] and mutually consistent results have been obtained to a certain degree. In addition, Bragg fibers were demonstrated and it was reported that they reveal the tolerance for bending loss [14,15]. In analytical approaches, the Bloch theorem was applied to the radially stratified cladding layers. In the cylindrical coordinates, however, the original Bloch theorem does not apply strictly. In previous works, instead, an asymptotic expansion approximation was employed [7–10]. In this approximation, cylindrical waves are described as the asymptotic expansion of cylindrical functions in the lowest order and are treated as nearly plane waves. In those studies, results are absolutely affected by the approximation accuracy in the Bloch theorem, therefore, the application range of the theory is restricted to the asymptotic region. For more accurate results, we need to apply the Bloch theorem in a better approximation.

In this paper, we study the description of the Bloch theorem in the cylindrical coordinates. In the present scheme, an approximation, though it has higher precision than previous one, is still used. However, the electromagnetic fields are genuinely treated as cylindrical waves, namely, the Bessel functions, instead of the asymptotic expansion. Then, we apply it to the Bragg fiber, and we show a method to obtain the propagation constant and electromagnetic fields of the TE mode which has the lower propagation loss among all the mode groups [16]. Although the accuracy of the present scheme remains restricted by the accuracy of the Bloch theorem, the mathematical structure of the Bragg fiber becomes much clearer than previous works. The present scheme gives us various physical aspects of Bragg fibers to understand them.

This paper is organized as follows. In Sec. II, the Bloch theorem in the cylindrical coordinates is studied. In Sec. III, we show the fundamental equations of the TE mode in the Bragg fiber. Then, we apply the Bloch theorem in cylindrical coordinates to the TE mode and the eigenvalue equations are derived in Secs. IV and V, respectively. In Sec. VI, we discuss the present scheme from various viewpoints, and Sec. VII is devoted to the conclusion.

II. BLOCH THEOREM IN THE CYLINDRICAL COORDINATES

Let us begin with the description of the Bloch theorem in the cylindrical coordinates. We consider the electromagnetic

*akira@se.ritsumei.ac.jp
†jsakai@se.ritsumei.ac.jp

field propagating to the z direction in a material, with the angular frequency ω. Here, β is the propagation constant, a characteristic parameter of the optical fibers. With a spatiotemporal factor $U_{tz}=\exp[i(\omega t-\beta z)]$, the field component parallel to the z direction is separated into

$$\psi_z = U_{tz}F(r)\exp(i\nu\theta), \tag{1}$$

where ν is the azimuthal mode number. We restrict ourselves to a case where ν is not so large, that is, $0 \leq \nu \lesssim 3$, which is sufficient for a practical use. The function $F(r)$ satisfies the Bessel differential equation, namely, the Maxwell equation in the cylindrical coordinates

$$\frac{d^2F(r)}{dr^2} + \frac{1}{r}\frac{dF(r)}{dr} + \left[\kappa^2(r) - \frac{\nu^2}{r^2}\right]F(r) = 0, \tag{2}$$

with the lateral propagation constant $\kappa(r)$. Introducing a function $\Phi(r) \equiv \sqrt{r}F(r)$ and disregarding minute terms equal to and smaller than r^{-2} under $(\kappa r)^2 \gg 1$, we find that the above equation is formally reduced to the equation of harmonic oscillator

$$\frac{d^2\Phi(r)}{dr^2} + \kappa^2(r)\Phi(r) = 0. \tag{3}$$

We assume that the material has a periodic structure along the r direction such as $\kappa(r+\Lambda)=\kappa(r)$, with the period Λ. In such a medium, $\Phi(r)$ and $\Phi(r+\Lambda)$ satisfies the same Eq. (3), that is

$$\Phi(r+\Lambda) = C(\Lambda)\Phi(r), \tag{4}$$

where $C(\Lambda)$ is a coefficient dependent on the period Λ. Repeating use of Eq. (4) results in a relationship $C(N\Lambda) = [C(\Lambda)]^N$ for an arbitrary integer N. This relationship allows us to express as $C(\Lambda)=\exp(-iK\Lambda)$ with a complex number K. If a system possesses the periodic boundary condition with adequately long periodicity as is the case of one-dimensional system, then $C(N\Lambda)=1$ is added [2], imposing that K must be real.

In the present cylindrical system that is bounded at the origin, one obtains

$$\Phi(r+\Lambda) = \exp(-iK\Lambda)\Phi(r), \tag{5}$$

with the Bloch wave number K that is a complex number. The relationship strongly implies that $\Phi(r)$ should be represented by

$$\Phi(r) = \exp(-iKr)u(r), \tag{6}$$

where $u(r)$ is a periodic function with the period Λ, namely, $u(r+\Lambda)=u(r)$. For the cylindrical electromagnetic field propagating in a periodic medium, the Bloch theorem is expressed as

$$\sqrt{r+\Lambda}F(r+\Lambda) = \exp(-iK\Lambda)\sqrt{r}F(r), \tag{7}$$

$$F(r) = \exp(-iKr)\frac{u(r)}{\sqrt{r}}, \tag{8}$$

corresponding to Eqs. (5) and (6), respectively. Note that $F(r)$ has a singular point at $r=0$ due to the factor $1/\sqrt{r}$. It comes from the fact that the periodic structure is bounded at the origin in the cylindrical representation, whereas a boundless periodic structure is supposed in the original Bloch theorem. However, the neighborhood of the origin is out of the cladding region to apply the Bloch theorem, which is guaranteed by the fact that a certain core radius is necessary for the propagation mode due to the guiding limit. This point will be discussed in Sec. VI A again.

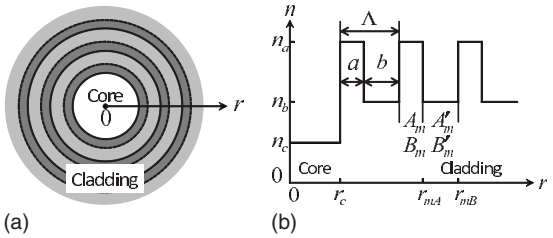

FIG. 1. The schematic of a Bragg fiber with a hollow core and alternate cladding layers a and b (left) and its refractive index distribution (right). a (b) is the thickness of the layer a (b) and $\Lambda=a+b$ is the period of the cladding layer. r_c is the core radius, $r_{mA}=r_c+(m-1)\Lambda+a$ and $r_{mB}=r_c+m\Lambda$ are the positions of interface at the mth layers a-b and the mth layer b-$(m+1)$th layer a, respectively. A_m, B_m (A'_m, B'_m) are the amplitude coefficients in the cladding layer a (b).

In Sec. IV, this cylindrical representation of Bloch theorem is applied to the TE mode in the Bragg fiber. Before that, we describe the fundamental equations of the TE mode in the following section.

III. FUNDAMENTAL EQUATIONS OF THE TE MODE IN THE BRAGG FIBER

The schematic of the Bragg fiber is shown in Fig. 1. The Bragg fiber has a hollow core and periodic cladding layers a and b with high and low refractive indices alternately. Now, we consider a situation that the TE mode of wavelength λ_0 propagates to the z direction inside the Bragg fiber. For the TE mode, the azimuthal mode number $\nu=0$. Then, the TE mode is characterized by H_z and E_θ,

$$\begin{pmatrix} H_z \\ iE_\theta \end{pmatrix} = U_{tz}D_i(r)\begin{pmatrix} A_i \\ B_i \end{pmatrix}, \tag{9}$$

where A_i and B_i are complex amplitude coefficients and

$$D_i(r) = \begin{pmatrix} H_0^{(2)}(\kappa_i r) & H_0^{(1)}(\kappa_i r) \\ -\dfrac{\omega\mu_0}{\kappa_i}H_0^{(2)\prime}(\kappa_i r) & -\dfrac{\omega\mu_0}{\kappa_i}H_0^{(1)\prime}(\kappa_i r) \end{pmatrix} \tag{10}$$

is the representation matrix for the ith layer. The index i is set to c for the core, a and b for the cladding layers a and b, respectively. Hankel functions $H_\nu^{(1)}=J_\nu+iY_\nu$ and $H_\nu^{(2)}=J_\nu-iY_\nu$ stand for the waves propagating inward and outward on a cross section, respectively. The prime indicates the differentiation with respect to the argument $\kappa_i r$. The lateral propagation constant for the ith layer is represented by

$$\kappa_i = [(n_i k_0)^2 - \beta^2]^{1/2}. \tag{11}$$

In addition, $k_0=\omega/c$, c, and μ_0 are the wave number, the light velocity, and the absolute permeability, respectively, in the vacuum.

For the sake of convenience, we introduce A_m, B_m (A'_m, B'_m) for the complex amplitude coefficients in the mth cladding layer a (b) instead of A_a, B_a (A_b, B_b). From the boundary condition at $r=r_c+(m-1)\Lambda+a\equiv r_{mA}$,

$$D_b(r_{mA})\begin{pmatrix} A'_m \\ B'_m \end{pmatrix} = D_a(r_{mA})\begin{pmatrix} A_m \\ B_m \end{pmatrix}, \tag{12}$$

and we obtain a sequence between amplitude coefficients of the mth layers a and b,

$$\begin{pmatrix} A'_m \\ B'_m \end{pmatrix} = D_b^{-1}(r_{mA})D_a(r_{mA})\begin{pmatrix} A_m \\ B_m \end{pmatrix} = \begin{pmatrix} f_{ab}(r_{mA}) & g_{ab}(r_{mA}) \\ g^*_{ab}(r_{mA}) & f^*_{ab}(r_{mA}) \end{pmatrix}\begin{pmatrix} A_m \\ B_m \end{pmatrix}, \tag{13}$$

where

$$f_{ij}(r) = \frac{i\pi\kappa_j r}{4}\left[\frac{\kappa_j}{\kappa_i}H_0^{(1)}(\kappa_j r)H_0^{(2)'}(\kappa_i r) - H_0^{(1)'}(\kappa_j r)H_0^{(2)}(\kappa_i r)\right], \tag{14}$$

$$g_{ij}(r) = \frac{i\pi\kappa_j r}{4}\left[\frac{\kappa_j}{\kappa_i}H_0^{(1)}(\kappa_j r)H_0^{(1)'}(\kappa_i r) - H_0^{(1)'}(\kappa_j r)H_0^{(1)}(\kappa_i r)\right]. \tag{15}$$

Here, we used Lommel's formula $H_\nu^{(1)}(z)H_\nu^{(2)'}(z) - H_\nu^{(1)'}(z)H_\nu^{(2)}(z) = -4i/\pi z$ [17] to calculate $D_b^{-1}(r_{mA})$. For the exchange of indices i and j in Eqs. (14) and (15), one obtains $f_{ji}(r)=(\kappa_i/\kappa_j)^2 f^*_{ij}(r)$ and $g_{ji}(r)=-(\kappa_i/\kappa_j)^2 g_{ij}(r)$, respectively. Using Lommel's formula again produces

$$|D_j^{-1}(r_{mA})D_i(r_{mA})| = |f_{ij}(r)|^2 - |g_{ij}(r)|^2 = \left(\frac{\kappa_j}{\kappa_i}\right)^2. \tag{16}$$

At $r=r_c+m\Lambda\equiv r_{mB}$, similarly, we have

$$\begin{pmatrix} A_{m+1} \\ B_{m+1} \end{pmatrix} = D_a^{-1}(r_{mB})D_b(r_{mB})\begin{pmatrix} A'_m \\ B'_m \end{pmatrix} = \begin{pmatrix} f_{ba}(r_{mB}) & g_{ba}(r_{mB}) \\ g^*_{ba}(r_{mB}) & f^*_{ba}(r_{mB}) \end{pmatrix}\begin{pmatrix} A'_m \\ B'_m \end{pmatrix}. \tag{17}$$

The combination of Eqs. (13) and (17) leads to a relationship between adjacent cladding layers a,

$$\begin{pmatrix} A_{m+1} \\ B_{m+1} \end{pmatrix} = \begin{pmatrix} X_m & Y_m \\ Y^*_m & X^*_m \end{pmatrix}\begin{pmatrix} A_m \\ B_m \end{pmatrix}, \tag{18}$$

where

$$X_m = f_{ba}(r_{mB})f_{ab}(r_{mA}) + g_{ba}(r_{mB})g^*_{ab}(r_{mA}), \tag{19}$$

$$Y_m = f_{ba}(r_{mB})g_{ab}(r_{mA}) + g_{ba}(r_{mB})f^*_{ab}(r_{mA}). \tag{20}$$

Since the coefficient matrix in Eq. (18) is the product of $D_a^{-1}(r_{mB})D_b(r_{mB})$ and $D_b^{-1}(r_{mA})D_a(r_{mA})$, we can find that it is a unimodular matrix, that is,

$$|X_m|^2 - |Y_m|^2 = [|f_{ba}(r_{mB})|^2 - |g_{ba}(r_{mB})|^2][|f_{ab}(r_{mA})|^2 - |g_{ab}(r_{mA})|^2] = 1, \tag{21}$$

where we used Eq. (16). This point will be discussed in Sec. VI B

IV. APPLICATION OF THE BLOCH THEOREM IN CYLINDRICAL COORDINATES TO THE TE MODE IN THE BRAGG FIBER

For the TE mode, the z component of the magnetic field in the mth cladding layer a is reduced to

$$H_z^{(m)}(r) = U_{tz}[A_m H_0^{(2)}(\kappa_a r) + B_m H_0^{(1)}(\kappa_a r)], \tag{22}$$

where we used the superscript m to specify the magnetic field in the mth layer. Substituting Eq. (22) into Eq. (7) at the most inner part of mth layer a, that is, $r=r_{(m-1)B}$,

$$\sqrt{r_{mB}}H_z^{(m+1)}(r_{mB}) = \exp(-i\tilde{K}\Lambda)\sqrt{r_{(m-1)B}}H_z^{(m)}(r_{(m-1)B}), \tag{23}$$

where $\tilde{K}$ is the Bloch wave number. An introduction of invertible matrices $\mathcal{M}_m$ leads the above relationship to the following equation:

$$\begin{aligned}\sqrt{r_{mB}}(H_0^{(2)}(\kappa_a r_{mB}), H_0^{(1)}(\kappa_a r_{mB}))\mathcal{M}_{m+1}\mathcal{M}_{m+1}^{-1}\begin{pmatrix} A_{m+1} \\ B_{m+1} \end{pmatrix} \\ = \exp(-i\tilde{K}\Lambda)\sqrt{r_{(m-1)B}}(H_0^{(2)}(\kappa_a r_{(m-1)B}), H_0^{(1)}(\kappa_a r_{(m-1)B})) \\ \times \mathcal{M}_m\mathcal{M}_m^{-1}\begin{pmatrix} A_m \\ B_m \end{pmatrix}.\end{aligned} \tag{24}$$

The matrices $\mathcal{M}_m$ are introduced to associate the mth with $(m+1)$th amplitude coefficients.

Let us choose matrices $\mathcal{M}_m$ so as to satisfy

$$\begin{aligned}&(H_0^{(2)}(\kappa_a r_{mB}), H_0^{(1)}(\kappa_a r_{mB}))\mathcal{M}_{m+1} \\ &= (H_0^{(2)}(\kappa_a r_{(m-1)B}), H_0^{(1)}(\kappa_a r_{(m-1)B}))\mathcal{M}_m \\ &= (C_1, C_2),\end{aligned} \tag{25}$$

where C_1 and C_2 are complex numbers independent of m. Now, we set

$$C_1 = C_2 = \sqrt{2/\pi\kappa_a} \tag{26}$$

so that $\sqrt{r_{(m-1)B}}\mathcal{M}_m^{-1}$ is equal to the transformation matrix $\tilde{U}_m$, introduced to relate the absolute coordinates with the relative coordinates discussed in Appendix A. Then we can see that a solution satisfying Eq. (25) is

$$\mathcal{M}_m = \sqrt{\frac{2}{\pi\kappa_a}} \begin{pmatrix} \dfrac{1}{H_0^{(2)}(\kappa_a r_{(m-1)B})} & 0 \\ 0 & \dfrac{1}{H_0^{(1)}(\kappa_a r_{(m-1)B})} \end{pmatrix}. \tag{27}$$

Employing Eq. (27), we obtain a relationship between the mth and $(m+1)$th amplitude coefficients

$$\begin{pmatrix} A_{m+1} \\ B_{m+1} \end{pmatrix} = \exp(-i\tilde{K}\Lambda)\Theta_{(m+1),m} \begin{pmatrix} A_m \\ B_m \end{pmatrix}, \tag{28}$$

where

$$\Theta_{m',m} = \sqrt{\frac{r_{(m-1)B}}{r_{(m'-1)B}}} \mathcal{M}_{m'} \mathcal{M}_m^{-1} = \begin{pmatrix} \vartheta_{11} & 0 \\ 0 & \vartheta_{22} \end{pmatrix} \tag{29}$$

and

$$\vartheta_{11} = \sqrt{\frac{r_{(m-1)B}}{r_{(m'-1)B}}} \frac{H_0^{(2)}(\kappa_a r_{(m-1)B})}{H_0^{(2)}(\kappa_a r_{(m'-1)B})},$$

$$\vartheta_{22} = \sqrt{\frac{r_{(m-1)B}}{r_{(m'-1)B}}} \frac{H_0^{(1)}(\kappa_a r_{(m-1)B})}{H_0^{(1)}(\kappa_a r_{(m'-1)B})}. \tag{30}$$

From this representation, we can derive a reduction formula on $\Theta_{m',m}$,

$$\Theta_{m'',m'}\Theta_{m',m} = \Theta_{m'',m}. \tag{31}$$

For $m''=m$, in particular, we obtain $\Theta_{m,m'} = \Theta_{m',m}^{-1}$. We can say that the transformation $\Theta_{m',m}$ forms a group. The transformation $\Theta_{m',m}$ for adjacent cladding layers reduces to the unit matrix in the previous picture [9], as will be discussed in Appendix A.

V. EIGENVALUE EQUATIONS FOR THE CYLINDRICALLY PERIODIC STRUCTURE

In this section, we connect two sequences of amplitude coefficients. One is obtained by the consideration of electromagnetic treatment in Sec. III and the other by the Bloch theorem in cylindrical coordinates in the preceding section. Equating right-hand sides of Eqs. (18) and (28) yields

$$\begin{pmatrix} X_m & Y_m \\ Y_m^* & X_m^* \end{pmatrix} \begin{pmatrix} A_m \\ B_m \end{pmatrix} = \exp(-i\tilde{K}\Lambda)\Theta_{(m+1),m} \begin{pmatrix} A_m \\ B_m \end{pmatrix}. \tag{32}$$

Premultiplication of $\Theta_{(m+1),m}^{-1}$ on both sides of Eq. (32) gives eigenvalues

$$\exp(-i\tilde{K}_j\Lambda) = \mathrm{Re}(\tilde{X}_m) \pm \{[\mathrm{Re}(\tilde{X}_m)]^2 - |\tilde{X}_m|^2 + |\tilde{Y}_m|^2\}^{1/2}, \tag{33}$$

where

$$\tilde{X}_m = \sqrt{\frac{r_{mB}}{r_{(m-1)B}}} \frac{H_0^{(2)}(\kappa_a r_{mB})}{H_0^{(2)}(\kappa_a r_{(m-1)B})} X_m, \tag{34}$$

$$\tilde{Y}_m = \sqrt{\frac{r_{mB}}{r_{(m-1)B}}} \frac{H_0^{(2)}(\kappa_a r_{mB})}{H_0^{(2)}(\kappa_a r_{(m-1)B})} Y_m, \tag{35}$$

and $j=1,2$ corresponds to the plus and minus signs, respectively, in the right-hand side of Eq. (33), the first eigenvalue equation. It depends upon the situation which eigenvalue ($j=1,2$) should be used, as shown in Appendix B. Note that $|\tilde{X}_m|^2 - |\tilde{Y}_m|^2 \approx 1$, although it is not exactly equal to unity. From Eq. (33), the Bloch wave number is dependent on the cladding ordering m in a strict sense. However, its dependence on m is so slight that we can treat $\tilde{K}_j$ as a constant, as will be clarified in Sec. VI A. Henceforth, we adopt $\tilde{K}_j$ at $m=1$ as the Bloch wave number.

The eigenvector corresponding to eigenvalues $\exp(-i\tilde{K}_j\Lambda)$ is

$$\begin{pmatrix} A_m \\ B_m \end{pmatrix} = \tilde{\xi}_m \begin{pmatrix} \tilde{Y}_m \\ \exp(-i\tilde{K}_j\Lambda) - \tilde{X}_m \end{pmatrix}, \tag{36}$$

where $\tilde{\xi}_m$ is an adjustment parameter and $\tilde{\xi}_1$ will be determined from the boundary condition at $r=r_c$ later. Using Eq. (28) repeatedly, we obtain the amplitude coefficients in the mth layer with those of the innermost cladding layer

$$\begin{pmatrix} A_m \\ B_m \end{pmatrix} = \tilde{\xi}_1 \exp[-i(m-1)\tilde{K}_j\Lambda]\Theta_{m,1} \begin{pmatrix} \tilde{Y}_1 \\ \exp(-i\tilde{K}_j\Lambda) - \tilde{X}_1 \end{pmatrix}, \tag{37}$$

where Eq. (31) is also considered.

To determine the amplitude coefficients in the innermost cladding layer, we consider the boundary condition at the core-cladding interface, $r=r_c$. An equality $B_c=A_c$ is necessary for securing that the electromagnetic wave must be finite at $r=0$. Therefore Eq. (9) for the core is reduced to

$$\begin{pmatrix} H_z \\ iE_\theta \end{pmatrix}_{r=r_c} = U_{tz} \begin{pmatrix} 2A_c J_0(\kappa_c r_c) \\ -2\dfrac{\omega\mu_0}{\kappa_c} A_c J_0'(\kappa_c r_c) \end{pmatrix}, \tag{38}$$

where A_c is an arbitrary constant. Use of the above representation results in

$$\begin{pmatrix} 2A_c J_0(\kappa_c r_c) \\ -2\dfrac{\omega\mu_0}{\kappa_c} A_c J_0'(\kappa_c r_c) \end{pmatrix} = D_a(r_c)\tilde{\xi}_1 \begin{pmatrix} \tilde{Y}_1 \\ \exp(-i\tilde{K}_j\Lambda) - \tilde{X}_1 \end{pmatrix}. \tag{39}$$

The above equation becomes

$$\begin{pmatrix} \zeta_{11} & \zeta_{12} \\ \zeta_{21} & \zeta_{22} \end{pmatrix} \begin{pmatrix} A_c \\ \tilde{\xi}_1 \end{pmatrix} = 0 \tag{40}$$

in a matrix form, where

$$\zeta_{11} = 2J_0(\kappa_c r_c),$$

$$\zeta_{12} = -\{H_0^{(1)}(\kappa_a r_c)[\exp(-i\tilde{K}_j\Lambda) - \tilde{X}_1] + H_0^{(2)}(\kappa_a r_c)\tilde{Y}_1\},$$

$$\zeta_{21} = \frac{2}{\kappa_c} J_0'(\kappa_c r_c),$$

$$\zeta_{22} = -\frac{1}{\kappa_a}\{H_0^{(1)\prime}(\kappa_a r_c)[\exp(-i\tilde{K}_j\Lambda) - \tilde{X}_1] + H_0^{(2)\prime}(\kappa_a r_c)\tilde{Y}_1\}. \tag{41}$$

In order that Eq. (40) may have nontrivial solutions, it is necessary and sufficient that the determinant of the coefficient matrix vanishes and the second eigenvalue equation of the TE mode is obtained as

$$\frac{J_0'(\kappa_c r_c)}{J_0(\kappa_c r_c)} + \frac{\kappa_c}{i\kappa_a}\tilde{\Sigma}_j = 0. \tag{42}$$

Here,

$$\tilde{\Sigma}_j = -i\frac{\sigma_j'(\kappa_a r_c)}{\sigma_j(\kappa_a r_c)} \tag{43}$$

and

$$\sigma_j(z) = H_0^{(1)}(z)[\exp(-i\tilde{K}_j\Lambda) - \tilde{X}_1] + H_0^{(2)}(z)\tilde{Y}_1. \tag{44}$$

The prime indicates the differential with respect to the argument. From Eq. (40), the ratio of amplitudes for the core and cladding is

$$\frac{\tilde{\xi}_1}{2A_c} = \frac{J_0(\kappa_c r_c)}{H_0^{(1)}(\kappa_a r_c)[\exp(-i\tilde{K}_j\Lambda) - \tilde{X}_1] + H_0^{(2)}(\kappa_a r_c)\tilde{Y}_1}. \tag{45}$$

Eigenvalue equations consist of Eqs. (33) and (42) which are analytically expressed in terms of the Bessel and Hankel functions unlike the previous works [7–10]. Solving these two equations simultaneously, we can calculate the propagation constant β, from which we can evaluate various properties. Reduction of the eigenvalue Eqs. (33) and (42) to the prior results [9] will be shown in Appendix A.

VI. DISCUSSION

In this section, we discuss some properties in the present scheme.

A. Consideration on the cylindrical Bloch theorem near the origin

It is described in Sec. II that the cylindrical Bloch theorem is guaranteed except for the vicinity of the origin. It will be shown here that this restriction does not prevent us from the application to the Bragg fiber. For the sake of easy understanding, we consider the quarter-wave stack (QWS) condition ($\kappa_a a = \kappa_b b = \pi/2$), where the Bragg diffraction occurs effectively in the cladding. This condition yields a simplified eigenvalue equation for an infinite number of the periodic cladding [10]

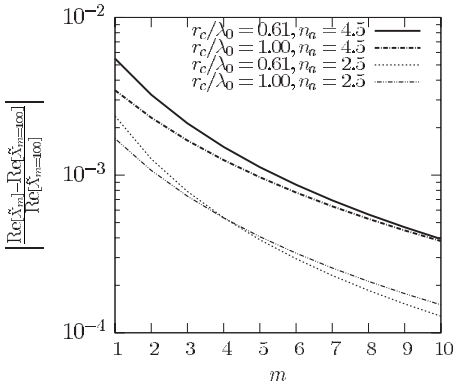

FIG. 2. The m dependence of relative difference of $\mathrm{Re}(\tilde{X}_m)$. Here, $\mathrm{Re}[\tilde{X}_{m=100}]$ is used as a reference since its deviation from the asymptotic value is negligible. The refractive indices of the layers a, b, and core are set to be n_a=4.5 and 2.5, n_b=1.5, and n_c=1.0. Other fiber parameters are determined such that they satisfy the quarter-wave stack condition for each case. The core radius is set to satisfy $r_c/\lambda_0 \geq U_{\mathrm{QWS}}/(2\pi n_c) \simeq 0.610$.

$$\kappa_c r_c = 2\pi\frac{r_c}{\lambda_0}\left[n_c^2 - \left(\frac{\beta}{k_0}\right)^2\right]^{1/2} = U_{\mathrm{QWS}}, \tag{46}$$

with $U_{\mathrm{QWS}} = j_{1,\mu}$ for the $\mathrm{TE}_{0\mu}$ mode and $j_{\nu,\mu}$ indicating the μth zeros of J_ν. Parameters such as the core radius r_c and thickness of cladding layers a and b should be decided in accordance with the QWS condition. Under the QWS condition, the TE mode is guided for $r_c/\lambda_0 \geq U_{\mathrm{QWS}}/(2\pi n_c)$. The minimum value of the lower guiding limit is 0.6098 given by the TE_{01} mode.

The Bloch wave number $\tilde{K}_j$ necessary for calculating the eigenvalue depends on the cladding ordering in a strict sense, as shown in Eq. (33). Since $|\tilde{X}_m|^2 - |\tilde{Y}_m|^2 \approx 1$, the $\tilde{K}_j$ is substantially a function of $\mathrm{Re}(\tilde{X}_m)$. The $\tilde{K}_j$ can be calculated by insertion of β, which is obtained from Eq. (46), into Eq. (33) which implicitly includes β. Figure 2 shows the m dependence of relative deviation of $\mathrm{Re}(\tilde{X}_m)$ from its asymptotic value for several r_c/λ_0, including the lower guiding limit because the $\mathrm{Re}(\tilde{X}_m)$ is inclined to converge to a certain value with increasing the m. Here, the refractive index of cladding layer a is set to be n_a=2.5 and 4.5, the latter of which is close to a practically used value [11,14]. Indices of the cladding layer b and core are fixed at n_b=1.5 and n_c=1.0, respectively. As the n_a increases under fixed values of n_b and n_c, the relative difference between m=1 and 100 increases and converges to a finite value. It is natural that the difference at m=1 is reduced with the increase in r_c/λ_0. For example, at r_c/λ_0=0.61, the relative difference for n_a=2.5 and 4.5 is less than 0.24% and 0.55%, respectively. The relative difference is negligibly small even for the worst case where n_a is infinite and r_c/λ_0=0.61 because it is 0.89% at m=1.

In summary, the Bloch wave number $\tilde{K}_j$ can be regarded as a constant independent of m even in the cylindrical Bloch theorem. This means that the restriction concerning the neighborhood of the origin in the cylindrical Bloch theorem imposes no substantial restriction on a practical use.

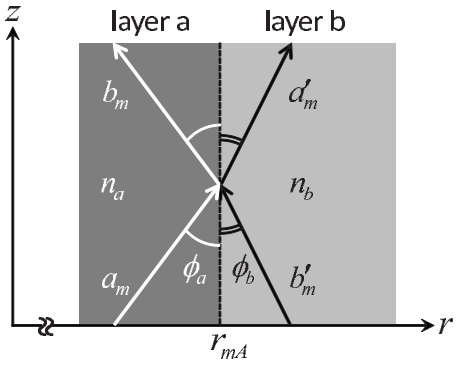

FIG. 3. Interface between the mth cladding layers a and b in an infinitesimal region. Outward rays a_m and a'_m and inward rays b_m and b'_m are coupled with each other on the interface at $r=r_{mA}$. ϕ_a and ϕ_b are the angles which a_m and b'_m make with respect to the interface, respectively. The magnitude of vectors corresponds to the wave number in medium.

B. Physical meanings of sequences between amplitude coefficients

In our description of electromagnetic waves, the Hankel functions of the first and second kinds stand for the waves propagating inward and outward, respectively. An expression given in Eq. (16) can also be obtained using geometrical optics as follows. Geometrical optics is valid for a limiting case of wavelength, $\lambda_0 \to 0$. This is equivalent to a condition, $\kappa_i r \gg 1$, which justifies an asymptotic expansion approximation used in Refs. [9,10]. The TE mode behaves as the meridional ray because its caustic radius becomes zero in the Bragg fiber [18], indicating that the ray can be considered in the r-z plane, as shown next.

In Fig. 3, the interface between the mth cladding layers a and b is illustrated. Let optical rays a_m and a'_m (b_m and b'_m) propagate outward (inward). According to the reflection law of ray, both a_m and b_m make an identical angle ϕ_a with respect to the interface at $r=r_{mA}$. The same is true of ϕ_b concerning the b'_m and a'_m. Four rays interact with each other on the interface. Here, these angles are measured from the axis parallel to the z direction according to the convention of fiber optics.

Let us associate each optical ray with a cylindrical wave. In the cladding layer $i(=a,b)$, the z component of magnetic field is described under the asymptotic expansion approximation as

$$H_z^{(i,m)} \propto \frac{1}{\sqrt{k_{i,r} r}}[a_m \exp(-ik_{i,r}r) + b_m \exp(ik_{i,r}r)], \quad (47)$$

where $(k_{i,r}, k_{i,\theta}, k_{i,z}) = (n_i k_0 \sin\phi_i, 0, n_i k_0 \cos\phi_i)$ is the wave-number vector of the outward ray a_m for the TE mode. When phase factors $\exp(-i\kappa_a r_{(m-1)B})$ and $\exp(i\kappa_a r_{(m-1)B})$ are included in amplitude coefficients a_m and b_m, respectively, Eq. (47) leads to the treatment in the previous picture [9]. For the layer b ($i=b$), the primed amplitude coefficients (a'_m, b'_m) are applied instead of (a_m, b_m). Another component of electromagnetic field along the θ axis is calculated to be

$$E_\theta^{(i,m)} \propto \frac{1}{\sqrt{(k_{i,r})^3 r}}[a_m \exp(-ik_{i,r}r) - b_m \exp(ik_{i,r}r)]. \quad (48)$$

From the continuity condition of electromagnetic fields at $r=r_{mA}$, we have the following relationship:

$$\begin{pmatrix} a'_m \\ b'_m \end{pmatrix} = \begin{pmatrix} \bar{f}_{ab} & \bar{g}_{ab} \\ \bar{g}^*_{ab} & \bar{f}^*_{ab} \end{pmatrix} \begin{pmatrix} a_m \\ b_m \end{pmatrix}, \quad (49)$$

where

$$\bar{f}_{ab} = \frac{1}{2}\sqrt{\frac{k_{b,r}}{k_{a,r}}}\left(1 + \frac{k_{b,r}}{k_{a,r}}\right)\exp[-i(k_{a,r} - k_{b,r})r_{mA}], \quad (50)$$

$$\bar{g}_{ab} = \frac{1}{2}\sqrt{\frac{k_{b,r}}{k_{a,r}}}\left(1 - \frac{k_{b,r}}{k_{a,r}}\right)\exp[i(k_{a,r} + k_{b,r})r_{mA}]. \quad (51)$$

It follows that $|\bar{f}_{ab}|^2 - |\bar{g}_{ab}|^2 = (k_{b,r}/k_{a,r})^2$. Relating $k_{i,r}$ to the lateral propagation constant as $\kappa_i = k_{i,r} = n_i k_0 \sin\phi_i$, we see that this relationship agrees with Eq. (16). On the other hand, the z component of the wave-number vector in each layer is identical with the propagation constant, $\beta = n_a k_0 \cos\phi_a = n_b k_0 \cos\phi_b$, which corresponds to Snell's law.

Rays a_m, a'_m, b_m, and b'_m correspond to the amplitude coefficients A_m, A'_m, B_m, and B'_m in the present representation, respectively. The factor $(k_{i,r})^{-1/2}$ in Eq. (47) is essential in the present cylindrical scheme. If this factor is not taken into account, which means that each ray is associated with a plane wave, then we arrive at a different result $|\bar{f}_{ab}|^2 - |\bar{g}_{ab}|^2 = k_{b,r}/k_{a,r}$.

Equations (13), (17), and (18) mean how each of waves is coupled with others. These sequences also describe the relationship of electromagnetic field intensities in each layer. Let us introduce the total flux $\mathcal{E}_m = |A_m|^2 - |B_m|^2$ ($\mathcal{E}'_m = |A'_m|^2 - |B'_m|^2$) in the mth layer a (b), taking the direction of propagation into account. Under the transformation (13), the total flux varies by the factor given in Eq. (16), that is, $\mathcal{E}'_m = (\kappa_b/\kappa_a)^2 \mathcal{E}_m$. In the present scheme, the total flux is proportional to the energy density in each cladding layer. When $n_a > n_b$, which means that the light velocity in the layer a is slower than in the layer b, the energy density in the mth layer a is higher than that in the mth layer a ($\mathcal{E}_m > \mathcal{E}'_m$) because $(\kappa_b/\kappa_a)^2 < 1$.

Equations (16) and (21) make it possible to design a new class of Bragg fibers which are composed of multiple kinds of cladding materials. For the mth and $(m+1)$th layers a, the relationship of total fluxes is calculated as $\mathcal{E}_{m+1} = \mathcal{E}_m$ from Eq. (21). It means that the energy density in layers of a kind is identical to each other in spite of a spatial separation and that the effect of layer between them, namely, layer b, disappears. For multilayer structures, similarly, total fluxes of arbitrary two layers are related with each other by the property of themselves only, independent of the structure between them. When the layer consists of A, B, and Γ, for example, we can see that the energy densities of layers A and Γ are related as $\mathcal{E}_\Gamma = (\kappa_\Gamma/\kappa_A)^2 \mathcal{E}_A$ from Eq. (16) without the effect of the layer B. In Fig. 4, we show variations of Bragg fiber with cladding consisting of three kinds of layers.

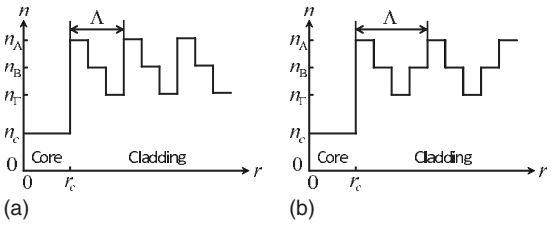

FIG. 4. Examples of the refractive index distribution of generalized Bragg fibers with three kinds of layers: asymmetric (left) and symmetric (right) in a period. Here, n_c and $n_i(i=\mathrm{A},\mathrm{B},\Gamma)$ are the refractive indices in the core and cladding layer i, respectively, and the cases of $n_\mathrm{A}>n_\mathrm{B}>n_\Gamma$ are indicated. In a period, three and four interfaces are contained, respectively. Inverted magnitude about n_B and n_Γ is also permitted.

C. Bloch theorem description in various coordinates

In the present scheme, we have applied the Bloch theorem to the cylindrical coordinates, which is applicable to other systems. Let us suppose that the wave function is separated into

$$\Phi(r;r_0)=\chi(r-r_0)F(r), \tag{52}$$

where $r_0=0$ is the origin of the radial direction and usually set to zero. A function χ is dependent on the radial position measured from the origin and is determined appropriately in accordance with coordinate systems. The function χ is strongly dependent on r_0, whereas $F(r)$ is little affected by r_0. It implies that $F(r)$ is approximately invariant under the translation operation by the period Λ, namely, $F(r+\Lambda)\approx F(r)$, except for the vicinity of the origin.

In the present scheme, namely, the cylindrical coordinates, $\chi(r-r_0)$ is set to $\sqrt{r-r_0}$. In the spherical coordinates, for example, this function should be chosen as $\chi(r-r_0)=r-r_0$ with which the Maxwell equation in the spherical coordinates is approximately reduced to the equation of harmonic oscillator again. These are consistent with the fact that the field intensity $|\Phi(r;r_0)|^2$ is attenuated by the ratio of $(r-r_0)^{-1}$ and $(r-r_0)^{-2}$ in each of coordinates, respectively. Note that the wave functions have a singular point at the origin for the cylindrical and spherical coordinates. The Cartesian coordinate system is a special case in which $\chi(r-r_0)$ should be unity. In this case, the dependence of wave function $\Phi(r;r_0)$ on the origin r_0 disappears, which is the situation supposed in the original Bloch theorem.

VII. CONCLUSION

We have studied the description of the Bloch theorem in the cylindrically periodic structure. This theorem is valid, in a good approximation, except for the neighborhood of the origin due to the singular point. The cylindrical Bloch theorem has been applied to the analysis of the TE mode in a Bragg fiber which consists of a hollow core and a multiannulus cladding. Numerical consideration on the Bragg fiber shows that the above exception imposes no substantial restriction on a practical use.

In the present scheme, the electromagnetic fields in the Bragg fiber are genuinely treated as the cylindrical waves, which provides us a clear mathematical model of the Bragg fiber. The eigenvalue equations are analytically expressed in terms of the Bessel and Hankel functions. The Bloch wave number can substantially be treated as a constant over the entire cladding region. The eigenvalue equations enable us to calculate the propagation constant and electromagnetic field distribution from which various characteristics can be derived with high accuracy.

Equations (16) and (21) are useful for understanding the physics in the Bragg fiber by combining with the concept of total flux, as described in Sec. VI B. Equation (16) is related with geometrical optics which is helpful for drawing the physical picture. These two equations give a criterion to design generalized Bragg fibers. It is shown that the Bloch theorem is applicable to coordinates other than cylindrical system, such as spherical coordinate system. Although the present scheme can be extended to the TM and hybrid modes, the work belongs to the future study.

APPENDIX A: CORRESPONDENCE BETWEEN PRESENT AND PREVIOUS PICTURES

Throughout this paper, cylindrical waves are described with Bessel functions and the absolute coordinate is used for radius variation. On the other hand, in the previous picture [9,10], the Hankel functions are approximated in the form of the asymptotic expansion, namely, nearly plane waves, and relative coordinates are introduced to calculate the phase factor in the cladding. In this appendix, we study the relationship between amplitude coefficients of these two pictures.

Let us introduce amplitude coefficients in the cladding layer a (b) for the previous picture as a_m, b_m (a'_m,b'_m), corresponding to A_m, B_m (A'_m,B'_m) in the present picture, respectively. From Eq. (9) in Ref. [9], the boundary condition at the interface of the mth cladding layers a and b $(r=r_{mA})$ is

$$G_bQ_b(r_{m,b}=0)\begin{pmatrix}a'_m\\ b'_m\end{pmatrix}=G_aQ_a(r_{m,a}=a)\begin{pmatrix}a_m\\ b_m\end{pmatrix}, \tag{A1}$$

where

$$G_i=\frac{1}{\sqrt{\kappa_i}}\begin{pmatrix}1 & 1\\ i\dfrac{\omega\mu_0}{\kappa_i} & -i\dfrac{\omega\mu_0}{\kappa_i}\end{pmatrix}, \tag{A2}$$

$$Q_i(r)=\begin{pmatrix}\exp(-i\kappa_i r) & 0\\ 0 & \exp(i\kappa_i r)\end{pmatrix}, \tag{A3}$$

and $0\le r_{a,m}\le a$ and $0\le r_{b,m}\le b$ are relative coordinates measured from $r=r_{(m-1)B}$ and r_{mA} in the absolute coordinate, respectively. On the other hand, the boundary condition in the absolute coordinate picture is represented by Eq. (12), the left-hand side of which can be equated to the left-hand side of Eq. (A1). With the asymptotic expansion of Hankel functions,

$$\begin{pmatrix}a_m\\ b_m\end{pmatrix}=\tilde{U}_m\begin{pmatrix}A_m\\ B_m\end{pmatrix}, \tag{A4}$$

where

$$\tilde{U}_m = \begin{pmatrix} \exp(-i\phi_m) & 0 \\ 0 & \exp(i\phi_m) \end{pmatrix} \tag{A5}$$

is a unitary matrix and $\phi_m = \kappa_a r_{(m-1)B} - \pi/4$.

Note that the total flux $\mathcal{E}_m$, defined in Sec. VI B, in both sides is invariant under the transformation $\tilde{U}_m$. In the asymptotic expansion, $\tilde{U}_m$ is proportional to the inverse matrix $\mathcal{M}_m^{-1}$. In the relative coordinate picture

$$\sqrt{r_{(m-1)B}}\mathcal{M}_m^{-1} = \tilde{U}_m(r_{a,m}=0) = 1, \tag{A6}$$

indicating that $\Theta_{(m+1),m}=1$ in this picture. With above, we have shown that Eq. (32) reduces to Eq. (18) in Ref. [9].

Premultiplying Eq. (18) by $\tilde{U}_{m+1}$ and making use of $\tilde{U}_m^\dagger \tilde{U}_m = 1$, we obtain

$$\begin{pmatrix} a_{m+1} \\ b_{m+1} \end{pmatrix} = \tilde{U}_{m+1} \begin{pmatrix} X_m & Y_m \\ Y_m^* & X_m^* \end{pmatrix} \tilde{U}_m^\dagger \begin{pmatrix} a_m \\ b_m \end{pmatrix} \simeq \begin{pmatrix} X & Y \\ Y^* & X^* \end{pmatrix} \begin{pmatrix} a_m \\ b_m \end{pmatrix}, \tag{A7}$$

where

$$X_m \exp[-i(\phi_{m+1} - \phi_m)] \simeq \left[\cos \kappa_b b - \frac{i}{2}\left(\frac{\kappa_b}{\kappa_a} + \frac{\kappa_a}{\kappa_b}\right)\sin \kappa_b b\right]\exp(-i\kappa_a a) = X, \tag{A8}$$

$$Y_m \exp[-i(\phi_{m+1} + \phi_m)] \simeq \frac{i}{2}\left(\frac{\kappa_b}{\kappa_a} - \frac{\kappa_a}{\kappa_b}\right)\sin \kappa_b b \exp(i\kappa_a a) = Y, \tag{A9}$$

and $|X|^2 - |Y|^2 = 1$. Hence, we have confirmed that Eq. (18) reduces to Eq. (12) in Ref. [9].

Then, we show the eigenvalue equations are consistently described under the transformation (A4). With the asymptotic expansion of Hankel functions,

$$\sqrt{\frac{r_{mB}}{r_{(m-1)B}}}\frac{H_0^{(2)}(\kappa_a r_{mB})}{H_0^{(2)}(\kappa_a r_{(m-1)B})} \simeq \exp(-i\kappa_a \Lambda), \tag{A10}$$

then $\tilde{X}_m \simeq X_m \exp(-i\kappa_a\Lambda) = X$. Therefore, eigenvalues $\exp(-iK_j\Lambda)$ are formally identical with each other in both pictures ($\tilde{K}_j \simeq K_j$). This means that Eq. (33) is in formal agreement with Eq. (19) in Ref. [9]. Furthermore, with $\tilde{Y}_m \simeq Y_m \exp(-i\kappa_a\Lambda) = Y \exp[i(\phi_{m+1} + \phi_m) - i\kappa_a\Lambda]$,

$$\tilde{\Sigma}_j \simeq \frac{[\exp(-iK_j\Lambda) - X] - Y}{[\exp(-iK_j\Lambda) - X] + Y}, \tag{A11}$$

then Eq. (42) is equivalent to Eq. (21) in Ref. [9].

As stated above, the representations in the present scheme are consistent with the results in Ref. [9].

APPENDIX B: RELATIONSHIP BETWEEN THE ELECTROMAGNETIC MODES AND BLOCH WAVE NUMBER IN BRAGG FIBER

In the present scheme, the electromagnetic fields in the Bragg fiber are associated with the Bloch wave number, as mentioned in Ref. [9]. Subtracting the complex conjugate of lower component in Eq. (18) from the upper component, we obtain

$$A_{m+1} - B_{m+1}^* = X_m(A_m - B_m^*) + Y_m(A_m^* - B_m). \tag{B1}$$

Since X_m and Y_m are generally nonzero, $B_m^* = A_m$ must hold for arbitrary m. The index m means the ordering of cladding layers and it implies that the cladding layers are supposed to be repeated infinitely in the present model. In such a situation, the reflectance at the interface between the mth and $(m+1)$th cladding layers is unity, which is referred to in Ref. [9]. In practice, m should be a finite number and some degrees of the propagating field go out of the core to the cladding region. Now, however, let us continue discussion as m being sufficiently large.

The relation of $B_m = A_m^*$ produces $\exp(i\tilde{K}_j^*\Lambda) = \exp(-i\tilde{K}_j\Lambda)$ for propagation modes. To prevent the power of the eigenvalue in Eq. (37) from divergence for sufficiently large m, the Bloch wave number should be related to the electromagnetic wave in the Bragg fiber. When $\mathrm{Re}(\tilde{X}_m)$ is larger (smaller) than $(|\tilde{X}_m|^2 - |\tilde{Y}_m|^2)^{1/2}$, the eigenvalue $\tilde{K}_2(\tilde{K}_1)$ should be employed so that the electromagnetic field decays in the cladding. On the other hand, when $[\mathrm{Re}(\tilde{X}_m)]^2 < |\tilde{X}_m|^2 - |\tilde{Y}_m|^2$, the electromagnetic field oscillates in the cladding, which corresponds to the radiation mode [9].

[1] F. Bloch, Z. Phys. **52**, 555 (1928).
[2] C. Kittel, *Introduction to Solid State Physics*, 7th ed. (John Wiley & Sons, New York, 1996).
[3] P. Yeh, A. Yariv, and E. Marom, J. Opt. Soc. Am. **68**, 1196 (1978).
[4] E. Yablonovitch, Phys. Rev. Lett. **58**, 2059 (1987).
[5] T. A. Birks, P. J. Roberts, P. St. J. Russell, D. M. Atkin, and T. J. Shepherd, Electron. Lett. **31**, 1941 (1995).
[6] P. St. J. Russell, J. Lightwave Technol. **24**, 4729 (2006).
[7] Y. Xu, R. K. Lee, and A. Yariv, Opt. Lett. **25**, 1756 (2000).
[8] Y. Xu, A. Yariv, J. G. Fleming, and S.-Y. Lin, Opt. Express **11**, 1039 (2003).
[9] J. Sakai and P. Nouchi, Opt. Commun. **249**, 153 (2005).
[10] J. Sakai, J. Opt. Soc. Am. B **22**, 2319 (2005).
[11] Y. Xu, G. X. Ouyang, R. K. Lee, and A. Yariv, J. Lightwave Technol. **20**, 428 (2002).
[12] S. G. Johnson, M. Ibanescu, M. Skorobogatiy, O. Weisberg, T. D. Engeness, M. Soljačić, S. A. Jacobs, J. D. Joannopoulos, and Y. Fink, Opt. Express **9**, 748 (2001).
[13] M. Ibanescu, S. G. Johnson, M. Soljačić, J. D. Joannopoulos, Y. Fink, O. Weisberg, T. D. Engeness, S. A. Jacobs, and M. Skorobogatiy, Phys. Rev. E **67**, 046608 (2003).

[14] Y. Fink, D. J. Ripin, S. Fan, C. Chen, J. D. Joannopoulos, and E. L. Thomas, J. Lightwave Technol. **17**, 2039 (1999).
[15] B. Temelkuran, S. D. Hart, G. Benoit, J. D. Joannopoulos, and Y. Fink, Nature (London) **420**, 650 (2002).
[16] J. Sakai, J. Opt. Soc. Am. B **24**, 9 (2007).
[17] *Handbook of Mathematical Functions*, edited by M. Abramowitz and I. A. Stegun (Dover, New York, 1965).
[18] J. Sakai, J. Opt. Soc. Am. B **23**, 1029 (2006).